

1 **Solar occultation measurement of mesospheric ozone by**
2 **SAGE III/ISS: Impact of variations along the line of sight**
3 **caused by photochemistry**

4

5 **Murali Natarajan¹, Robert Damadeo¹, David Flittner¹**

6 ¹ Science Directorate, NASA Langley Research Center, 21 Langley Blvd., Mail Stop 401-B,
7 Hampton, VA 23681, USA.

8 Correspondence to: Murali Natarajan (murali.natarajan@nasa.gov)

9

10 **Abstract.** Twilight gradients in the concentration of atmospheric species with short
11 photochemical lifetimes influence the transmission data obtained in a solar occultation
12 instrument like the Stratospheric Aerosol and Gas Experiment III aboard the International Space
13 Station (SAGE III/ISS). These photochemically induced changes result in nonlinear asymmetries
14 in the species distribution near the tangent altitude along the line of sight (LOS). The bias
15 introduced by neglecting the effects of twilight variations in the retrieval of mesospheric ozone is
16 the focus of this study. O₃ in the mesosphere exhibits large variations near the terminator during
17 sunrise and sunset based on current understanding of the photochemistry of this altitude region.
18 The algorithm used in the SAGE III/ISS standard retrieval procedure for mesospheric ozone does
19 not include the effects of these gradients. This study illustrates a method for implementing a
20 correction scheme to account for the twilight variations in mesospheric O₃ and gives an estimate
21 of the **bias** in the standard retrieval. We use the results from a diurnal photochemical model

Deleted: error

23 conducted at different altitudes to develop a database of ratios of mesospheric O₃ at different
24 solar zenith angles (SZA) around 90° to O₃ at a SZA of 90° for both sunrise and sunset
25 conditions. These ratios are used to scale the O₃ at levels above the tangent altitude for
26 appropriate SZA in the calculation of the optical depth along the LOS. In general, the impact of
27 the corrections due to twilight variations is to increase the contribution of the overlying layers to
28 the optical depth thereby reducing the retrieved O₃ concentration at the tangent altitude. We find
29 that at sunrise the retrieved mesospheric O₃ including the diurnal corrections is lower by more
30 than 30% compared to the archived O₃. We show the results obtained for different latitudes and
31 seasons. In addition, for nearly colocated sunrise and sunset scans, we note that these corrections
32 lead to better qualitative agreement in the sunrise to sunset O₃ ratio with the photochemical
33 model prediction.

Deleted: zenith angles

Deleted:

Deleted: zenith angle

Deleted: zenith angles

Deleted: 2

Deleted: -

35 1 Introduction

36
37 The solar occultation measurement technique has been the workhorse among various methods
38 used for monitoring the composition of the earth's atmosphere for over 4 decades. This is
39 evidenced by many successful experiments such as SAGE, SAGE II, Halogen Occultation
40 Experiment (HALOE), Atmospheric Trace Molecule Spectroscopy (ATMOS), Atmospheric
41 Chemistry Experiment – Fourier Transform Spectrometer (ACE-FTS), Polar Ozone and Aerosol
42 Measurement (POAM), SAGE III/M3M and SAGE III/ISS. Major advantages of this technique
43 include high signal to noise ratio, high vertical resolution, and long-term accuracy provided by
44 the 'self-calibrating' nature of the instrument operation. Limited global coverage ranks high
45 among the disadvantages of this method. In the occultation experiments, the absorption of solar

Deleted: longer path length,

53 radiance measured by the instrument as a function of tangent height altitude or pressure is related
54 to the optical depth and hence the abundance of the species along the line of sight (LOS). The
55 bulk of the absorption, in general, occurs around the tangent point because of the exponential
56 decrease in atmospheric density with altitude and due to the slant path determined by the
57 spherical geometry. Algorithms used in standard retrievals assume that the species distribution in
58 atmospheric layers is homogeneous and, therefore, the variation along the LOS is symmetrical
59 around the tangent point location. The column along the LOS is then made up of species
60 concentrations at the tangent altitude and the layers above corresponding to a SZA of 90°. This
61 assumption is quite valid for species such as CH₄, H₂O, and stratospheric O₃ because of their
62 long photochemical lifetimes and the absence of chemically induced diurnal variations. In the
63 case of species with short lifetimes, the sudden changes in the photolysis rates near day/night
64 terminator trigger rapid variations in the concentration as a function of SZA. These variations
65 result in nonlinear asymmetry along the LOS. In this case, the column along the LOS is made up
66 of species concentration at a SZA of 90° at the tangent altitude and those from the layers above
67 at SZA different from 90° on either side of the tangent point.

Deleted: Standard a

Deleted: the

Deleted: distribution

Deleted: zenith angle

68
69 The influence of twilight variations in NO and ClO on the interpretation of solar occultation
70 measurements was described by Boughner et al. (1980). Correction factors based on
71 photochemical models, as discussed in the above study, have been routinely applied in the
72 retrievals of stratospheric NO and NO₂ profiles in HALOE (Gordley et al., 1996; Russell et al.,
73 1988) and in ATMOS (Newchurch et al., 1996). Brohede et al. (2007) described the role of
74 diurnal variations in the retrieval of NO₂ from OSIRIS measurements. The algorithm used in the
75 retrieval of NO₂ in SAGE, SAGE II, SAGE III/M3M, and SAGE III/ISS neglects the twilight

80 variations. [A recent study of the NO₂ retrieval from SAGE III/ISS by Dubé et al. \(2021\)](#)
81 describes the importance of considering the diurnal variations along the LOS.
82
83 Mesospheric O₃ is also characterized by short photochemical lifetimes and steep twilight
84 gradients and, therefore, it is a potential candidate species requiring appropriate corrections in a
85 retrieval from solar occultation instruments. Natarajan et al. (2005) noted that the diurnal
86 correction factors used in the retrieval of mesospheric ozone from HALOE (Version 19) needed
87 to be updated. They derived [new factors](#) from a diurnal photochemical model of mesospheric
88 ozone [and](#) illustrated the impact of the corrections using a small subset of retrieved HALOE
89 mesospheric O₃ profiles. In the present study, we describe the application of similar corrections
90 to the SAGE III/ISS retrieval of mesospheric O₃. Table 1 of the Data Product User's Guide for
91 SAGE III/ISS (2021) lists the release status of mesospheric O₃ data as a Beta version that is yet
92 to be validated, because it is still potentially impacted by spectral stray light within the
93 instrument. Our goal is to quantify the impact of the corrections on the archived data and to see
94 whether the changes can support other known criteria. A description of the mesospheric O₃
95 variations under twilight conditions as calculated with a diurnal photochemical model is given in
96 section 2. The occultation geometry and the diurnal correction factors for mesospheric O₃ are
97 described in section 3. Results from the application of the factors to correct the archived data are
98 discussed in section 4. We also include the results from an approximate retrieval using the
99 archived transmission data with and without diurnal corrections. [A comparison of zonally
100 averaged O₃ profiles with scaled data for the same period from the Microwave Limb Sounder
101 \(MLS\) instrument on Aura satellite is described in the next section. This is followed by a
102 discussion of sunrise to sunset mesospheric O₃ ratios using appropriate colocated scans and a](#)

Deleted: R
Deleted: c

Deleted: new factors were

Deleted: . They

Deleted: This

Deleted: -

109 comparison to theoretical values. The final summary section reiterates the importance of
110 corrections for photochemically induced twilight mesospheric O₃ variations in solar occultation
111 retrievals.

112

113 2 Mesospheric O₃ variations at sunrise/sunset

114

115 We use a time-dependent, one-dimensional photochemical model to obtain the diurnal variation
116 in mesospheric O₃. A detailed description of the model used in this study is given in Natarajan et
117 al. (2005). This version of the model extends from 56 km to 100 km at 1 km intervals. The
118 photochemical reaction scheme, shown in the appendix, includes reactions involving species
119 from the Oxygen, Hydrogen, and Nitrogen families. Chlorine and Bromine reactions do not play
120 a significant role in this region of the atmosphere. The adopted chemical rate constant data are
121 from the JPL Publication 19-5 (2020). The diurnal model does not use a family approximation
122 and reactive species O, O₃, N, NO, NO₂, H, OH, HO₂, and H₂O₂ are considered as independent
123 variables. The concentrations of long-lived species are constrained by the results from a two-
124 dimensional chemical transport model (CTM) (Callis et al., 1997). Diffusion coefficients from
125 the CTM are used to parameterize the vertical transport. The model is run for 4 diurnal cycles so
126 that the reactive species reach a steady diurnal behavior, and the results from the fifth cycle are
127 used in the analysis. The model is run for every month at 11 latitudes, corresponding to the
128 latitude nodes of the CTM, from 56.25° N to 56.25°S at an interval of 11.25°.

129

130 Calculated O₃ diurnal variation in June at the latitude of 11.25°S and at different altitudes of
131 interest to this work is illustrated in Figure 1. We are restricting our attention to altitudes below

Deleted: Diurnal variations in reactive species can be obtained using a time-dependent diurnal photochemical model. A detailed description of the model used in this study is given in Natarajan et al. (2005). For the present study, we have updated the chemical rate constant data using the JPL Publication 19-5 (2020).

Deleted: diurnal

139 74 km because the SAGE III/ISS O₃ data are noisy in the region above and the quoted
140 uncertainty is also large. O₃ concentration is shown as a function of time starting at midnight.
141 The upper X-axis shows the corresponding SZA. Nighttime O₃ has a constant value representing
142 the total odd oxygen in the lower mesosphere. A sharp decrease at sunrise is mainly caused by
143 photolysis of O₃ forming atomic oxygen. The recombination of atomic oxygen and O₂ quickly
144 balances the loss of O₃ from photolysis. This reaction is pressure dependent and becomes slower
145 at higher altitudes. The photolysis of O₂ generates additional odd oxygen (O_x = O + O₃) and in
146 the morning hours this leads to an increase in both O_x and O₃. The formation of odd hydrogen
147 species from the reaction of O(¹D) with H₂O during the day triggers the catalytic destruction of
148 odd oxygen through reactions involving OH. It is noted that between 50 and 80 km the chemical
149 time constant of O_x is of the order of few hours and O_x exhibits a diurnal variation caused by the
150 competing production and destruction reactions. In the early morning there is a net gain of O_x
151 and in the evening there is net loss of O_x which continues even after sunset until atomic oxygen
152 is depleted. The partitioning of O_x into O and O₃ is mainly controlled by the photolysis of O₃
153 and the production of O₃ through the recombination of O and O₂. The large increase in O₃ seen
154 around sunset is mainly due to the decrease in the photolysis of O₃ and the continuation of the
155 recombination of O and O₂. O₃ reaches a steady value within an hour or so after sunset. The
156 diurnal model extends to 100 km; however, since the quoted uncertainty above 70 km in the
157 archived SAGE III/ISS O₃ is large, we will focus on the region below.
158
159 The results of the full diurnal cycle are of general interest about the model simulation. But, with
160 reference to solar occultation measurements, the sharp gradients seen in the O₃ concentration
161 near SZA of 90° are more critical. The significance of the twilight variations to the retrieval of

Deleted: (1D)

Deleted: in this altitude range odd oxygen itself has a daytime ...

Deleted: evening

Deleted: fter

Deleted: recombination of atomic oxygen

Deleted: . At higher altitudes, not shown here, model predictions indicate a dramatic shift in the diurnal behavior of O₃.

Deleted: 70 km

Deleted: a zenith angle

173 mesospheric O₃ under sunrise/sunset conditions can be understood with the help of the schematic
174 shown in Figure 2. This illustrates the occultation geometry in the plane containing the LOS.
175 The red line denotes the LOS at a tangent altitude of Z_T. Points F and N represent the
176 intersection of the LOS with an atmospheric layer at an altitude of Z shown in green. For a
177 species with little or no twilight variations, the concentrations at the locations F and N are nearly
178 equal to that at the location U, the tangent point at an altitude of Z. In this case, the
179 concentrations at tangent height Z_T can be derived in a straightforward manner from the
180 measured transmission using a retrieval algorithm. However, if the photochemistry causes
181 significant gradients near SZA of 90°, as in the case of mesospheric O₃, the distribution around
182 the tangent point becomes nonlinearly asymmetric because the concentrations at F and N depend
183 on the respective local SZA. This variation must be incorporated in the evaluation of O₃ specific
184 optical depth along the LOS.

Deleted: zenith angles

185

186 To illustrate the impact of diurnal variations on slant-path column of O₃, we selected a typical
187 event from the SAGE III/ISS data and applied the calculated O₃ variations in the slant-path
188 column evaluation. The required parameters include month, date, event type (sunrise or sunset),
189 tangent altitude, latitude, longitude, spacecraft latitude and longitude. These data are taken from
190 the current Version 5.2 SAGE III/ISS data available from the Atmospheric Sciences Data Center
191 (ASDC) at NASA Langley Research Center. We used the model results for June at 11.25°S
192 latitude to get the O₃ at sunrise variation along the LOS corresponding to different tangent
193 altitudes from 56 to 76 km. The latitude of the chosen SAGE III/ISS measurement is 11.35°S.
194 The results for tangent altitude of 64 km are shown in the left panel of Figure 3. The X-axis
195 shows the distance along the LOS relative to the tangent point with positive direction towards

Deleted: aRC

198 instrument and negative direction towards the Sun. Corresponding SZAs are shown at the top.
199 The dotted line corresponds to the O₃ concentration along the LOS when the diurnal variations
200 are neglected and only the values corresponding to 90° SZA from the layers above the tangent
201 altitude are used. The solid line represents the O₃ including the diurnal variations at the
202 respective altitudes. The increased O₃ concentrations on the instrument side of the LOS are
203 readily seen. The ratio of the O₃ column along the LOS with diurnal variations to the column
204 without the diurnal variations is shown as a function of tangent altitude in the panel on the right
205 side. The peak difference of the order of 30% occurs in the altitude range from 61 to 72 km.
206 Underestimation of the partial O₃ slant-path column from layers above the tangent altitude in the
207 standard retrieval translates to overestimation of the retrieved O₃ at the tangent altitude. The bias
208 introduced by the neglect of twilight variations can be evaluated with the help of the diurnal
209 model results.

Deleted: zenith angles

Deleted: zenith angle

Deleted: is

Deleted: .

Deleted: error

Deleted: committed

210
211 The technique is to express the O₃ variation as a function of SZA in terms of concentration
212 normalized to O₃ at SZA of 90°. Figure 4 shows the distribution of the ratio $O_3(\theta)/O_3(\theta=90^\circ)$
213 near sunrise as a function of SZA and altitude obtained from the model results for 11.25°S
214 latitude in June. For a given tangent height, the total slant-path O₃ column comprises of partial
215 slant-path columns corresponding to the layers at and above the tangent height. Spherical
216 geometry dictates that the partial pathlength along the LOS is maximum for the layer
217 immediately above the tangent height (i.e., the lowest layer) and decreases dramatically for
218 higher layers. This, combined with decreasing O₃ concentration with height in the lower
219 mesosphere, results in a total slant-path column dominated by contributions from a few layers
220 right above the tangent point. Therefore, only a small range of SZA, say between 86° and 94°,

Deleted: zenith angle

Deleted: a

Deleted: zenith angle

Deleted: zenith angle

Deleted: zenith angles

232 centered at 90° are important. At 62 km the O₃ ratio is less than 1.0 for SZA less than 90° and it
233 increases gradually for SZA greater than 90°. At higher altitudes, the ratio shows a much steeper
234 increase for SZA greater than 92°. The ratio, in some cases, is even slightly larger than 1.0 at
235 SZA less than 90°. From the occultation geometry shown in Figure 2, it is seen that as one
236 moves away from a SZA of 90° along the LOS at any tangent altitude, the corresponding altitude
237 layer of interest moves upwards. Figure 5 illustrates the O₃ twilight ratio as a function of SZA
238 and altitude for sunset conditions for the same latitude and month. The changes in the ratio for
239 sunset condition are smaller and more gradual especially for SZA greater than 90° compared to
240 the sunrise case. It should be recalled that the daytime variation in the odd oxygen concentration
241 in the lower mesosphere impacts the O₃ concentration differently at sunrise and sunset. The
242 differences between the O₃ variations for sunrise and sunset conditions suggest that the effects on
243 the retrievals are different for sunrise and sunset occultations. The twilight O₃ ratios for altitude
244 layers above the tangent altitude can be used to get the O₃ concentration and hence the optical
245 depth along the LOS more accurately.

246
247 Mesospheric O₃ concentrations are influenced by reactions involving HO_x species and therefore
248 the distribution of H₂O used in the model is an important factor. An earlier study with HALOE
249 mesospheric O₃ data (Natarajan et al. 2005) using the results from the same CTM showed that
250 the monthly, zonal mean H₂O distribution from the CTM was in good agreement with the data
251 taken from the UARS reference atmosphere project. Linear trend in mesospheric H₂O and solar
252 cycle response have been addressed in literature (Remsberg et al., 2018; Yue et al., 2019). Yue
253 et al. (2019) report a trend in mesospheric H₂O of the order of 4 to 6% per decade based on the
254 data from the Sounding of the Atmosphere using Broadband Emission Radiometry (SABER) and

Deleted: zenith angle

Deleted: zenith angles

Deleted: zenith angles

Deleted: zenith angles

Deleted: zenith angle

Deleted: zenith angle

Deleted: zenith angles

Deleted: ,

263 MLS instruments. Long term variability in H₂O certainly impacts the absolute level of
264 mesospheric O₃. But, for the present study, the factor of importance is the relative variation of
265 O₃ very close to SZA of 90° during sunrise and sunset in the mesosphere. We have done a
266 sensitivity study at 11.25° S in June using the diurnal model with a 25% increase in the H₂O
267 concentration. Figure 6 displays the percent change in the twilight O₃ ratios for sunrise shown in
268 Figure 4. The maximum impact below 74 km is less than 20% and it is very small in the lower
269 regions. The twilight ratio in O₃ is quite robust and small changes in the atmospheric parameters
270 such as temperature and H₂O do not impact this ratio much. The use of this ratio is a valid
271 approximation in correcting the retrieval scheme.

Deleted: showed that the

Deleted: is

273 **3 SAGE III/ISS Mesospheric ozone**

274
275 The Sage III/ISS instrument payload was launched in February 2017 and successfully attached to
276 the ISS. The ISS occupies a low earth orbit at an inclination of 51.64° that provides occultation
277 coverage of low- and mid-latitude regions. Description of the experiment and early validation of
278 the O₃ measurements are given in McCormick et al. (2020) and Wang et al. (2020). More
279 detailed information on the various wavelength channels and data used for retrieving a suite of
280 atmospheric species including mesospheric O₃ are given in SAGE III Algorithm Theoretical
281 Basis Document (ATBD, 2002) and in the SAGE III/ISS Data Products User's Guide Version
282 3.0 (2021) (DPUG). Among the three different O₃ profile measurements made by the instrument,
283 the one based on short wavelengths in the Hartley-Huggins bands refers exclusively to
284 mesospheric O₃. Three Charge-Coupled Device (CCD) pixel groups (PGs 0-2) are assigned to
285 the short wavelengths in the 280 – 293 nm range, though only one (PG 1 centered at 286 nm) is

288 currently used for the retrieval. According to the DPUG, mesospheric O₃ data have not been
289 fully validated. We also note that the uncertainty in the archived O₃ concentration becomes
290 larger than 10% above 70 km and there are some spurious negative data pointing to uncertainties
291 in the transmission. The present study focusses only on SAGE III/ISS O₃ in the lower
292 mesosphere up to an altitude of 70 km even though the retrieval itself starts at 90 km. The
293 diurnal model described in the previous section extends up to 100km. We use the Version 5.2
294 transmission and species data obtained from ASDC at NASA LaRC. For each year and month,
295 we have categorized the scans according to event type, sunrise, or sunset. The input data for our
296 analysis include the tangent point latitude and longitude, spacecraft latitude and longitude,
297 vertical profiles of neutral density, mesospheric O₃, and transmission. We use only the
298 transmission data from the science pixel group 1 (PG1), which has a center wavelength of
299 286.124 nm, since the predominant species active in this wavelength region is O₃.

300

301 ~~We have generated a~~ database of O₃ twilight ratios for sunrise and sunset conditions ~~from the~~
302 diurnal model results. These ratios cover for each month the latitude range from 56.25°N to
303 56.25°S at an interval of 11.25°, ~~SZA~~ from 84° to 96° at 0.5° intervals, and altitudes from 56 to
304 90 km at 0.5 km intervals. Using the input data from each of the SAGE III/ISS occultations and
305 spherical geometry relations, for every tangent altitude ~~we compute the SZA~~ as well as partial
306 pathlengths corresponding to overlying layers. This generates a pathlength matrix like the one
307 used in the standard retrieval. Appropriate O₃ twilight ratios are then obtained by interpolation
308 using the ~~SZA~~ and layer altitude. Multiplication of the standard pathlength matrix by the O₃
309 ratios yields the modified pathlength matrix including the effects of diurnal variations.

310

Deleted: A

Deleted: has been generated

Deleted: zenith angles

Deleted: ,

Deleted: zenith angles

Deleted: zenith angle

317 The twilight ratios can either be used to modify the O₃ profiles from the standard retrieval or be
318 incorporated in a new retrieval from measured transmission profile. The first method is like the
319 procedure described by Dubé et al. (2021) for making diurnal corrections to stratospheric NO₂
320 data from SAGE III/ISS. The archived SAGE III/ISS O₃ profile and the standard pathlength
321 matrix are used to recreate the O₃ specific slant optical depth, as shown by the equation

$$322 \quad \tau = \sigma S n, \quad (1)$$

323 where τ is the O₃ slant optical depth profile, σ is the O₃ cross section corresponding to the center
324 wavelength of PG1, and n is the O₃ profile from the standard retrieval. S represents the
325 pathlength matrix with each row corresponding to a tangent point altitude. This can be written as
326 a triangular matrix because of the geometric symmetry on opposite sides of the tangent point as
327 can be seen from Figure 2. The slant optical depth can then be converted to a O₃ vertical profile
328 corrected for diurnal variations using the modified pathlength matrix described earlier, as shown
329 by the equation

$$330 \quad n_{wd} = (S_{wd})^{-1} \tau / \sigma = (S_{wd})^{-1} S n \quad (2)$$

331 where S_{wd} is the modified pathlength matrix with diurnal correction and n_{wd} is the corrected O₃
332 profile. Here it is assumed that the O₃ absorption coefficient remains constant along the LOS.

333 This procedure gives a quantitative estimate of the over-prediction by the standard retrieval. The

334 results for a sunrise event on June 14, 2021 (Event ID =2021061438SR) are shown in Figure 7.
335 The left panel displays the O₃ concentration profiles – the solid red line is the archived data from
336 standard retrieval and the solid black line represents the profile after applying the diurnal
337 correction ratios to the pathlength matrix. The percent difference between the standard and the
338 modified profiles is shown by the solid line on the right panel. For this occultation, the difference
339 exceeds 40% above 64 km. This is consistent with the change in O₃ slant column due to the

Deleted: e

Deleted: 6

342 diurnal correction shown in Figure 3. The right panel in Figure 3 shows around 30% increase in
343 the slant-path column between 61 and 72 km. We also note that the retrieval becomes noisy in
344 the upper altitudes as O₃ concentrations reach near detection limits. In the second method,
345 instead of evaluating the slant optical depth using equation 1, the archived slant-path
346 transmission data, which corresponds to PG1, is used along with the standard and modified
347 pathlength matrices to retrieve the vertical O₃ profiles. The change in the slant-path transmission
348 corresponding to the science CCD channel PG1 for each tangent altitude below an upper
349 boundary of 90 km is related to the total slant optical depth made up mainly of O₃ absorption and
350 Rayleigh scattering contributions. After removing the Rayleigh scattering part corresponding to
351 the center wavelength of 286.124 nm, the slant-path O₃ column can be estimated using the O₃
352 absorption coefficient at this wavelength taken from Bogumil et al. (2003), which is the same
353 database used in the SAGE retrieval algorithm. The standard and modified pathlength matrices
354 are then used to get the vertical O₃ profiles without and with corrections for diurnal variations
355 respectively. The retrieved O₃ profiles for the sunrise event mentioned earlier are given by the
356 dashed lines on the left panel of Figure 7, the red color denoting the standard retrieval without
357 diurnal corrections and the black color the modified retrieval with diurnal corrections. We have
358 used a very simple algorithm and assumed that the transmission data corresponds to a single
359 wavelength to simplify the calculation. The actual retrieval procedure used for the archived
360 products may have included more refinements. The agreement between results of the two
361 different methods is very good, both for the vertical O₃ profiles and for the percent differences.
362 Results for a sunset event, closer to the above sunrise event in location and within a day (Sunset
363 event ID = 2021061515SS) are shown in Figure 8. The impact of the diurnal correction is much
364 smaller for sunset conditions. The maximum difference between the standard and modified

Deleted:

Deleted: both

Deleted: variations

Deleted: 6

Deleted: 7

370 profiles is less than 10%. The two different procedures for incorporating diurnal effects yield
371 very nearly same results.

372

373 We have applied the diurnal corrections following the procedure described above to all the
374 SAGE III/ISS measurements from June 2021, categorized by the event type of sunrise or sunset.
375 Individual O₃ profiles were grouped together in 11 latitude bands, 11.25° wide between 56.25°N
376 and 56.25°S. The percent difference between the standard retrieval profile and the corresponding
377 modified profile, defined as $(O_3/O_{3, WD} - 1) * 100$, was calculated and the mean for each latitude
378 band was evaluated. The subscript WD refers to the retrieval including the diurnal corrections.

379 Figure 9 shows the resulting distribution of the mean, which represents the over-estimation by
380 the standard retrieval, as a function of latitude and altitude. There is a latitudinal dependence
381 with peak values occurring near 64 km and the summer hemisphere showing smaller difference.
382 Values higher than 100% (dark violet region) are seen in the upper altitudes of the winter
383 hemisphere. The O₃ profile has a sharp gradient reaching a very low minimum in winter between
384 and 70 and 80 km. The retrieved data in this region are very noisy and thus sometimes include
385 negative concentrations. The percent difference between the two retrievals also displays a very

386 noisy distribution with large values of both signs. At altitudes above 85 km, the day-night
387 terminator occurs at solar SZA greater than 96° and O₃ variation around 90° is small. The bias in
388 the standard retrieval (not shown) is also small and there is no need for diurnal correction. The
389 distribution of percent differences for sunset measurements is shown in Figure 10. The values are
390 much smaller as discussed earlier, since the diurnal corrections are not significant for sunset. To

391 look at the seasonal dependence of the impact of diurnal corrections on the retrieved O₃, we have
392 repeated the procedure with SAGE III/ISS data from January 2021. Figure 11 displays the results

Deleted: 8

Deleted: Near the upper boundary of 90 km, the data is smooth, and the bias caused by the diurnal variations is very small. ...

Deleted: these high altitudes,

Deleted: higher

Deleted: zenith angles

Deleted: the

Deleted: 9

Deleted: 0

403 for sunrise conditions. The differences between the standard and modified retrievals are larger
404 again in the winter hemisphere with peak values occurring near 64 km. This agrees qualitatively
405 with Figure 11 of Natarajan et al. (2005), which showed the percent difference in retrieved
406 HALOE sunrise O₃ for January 1995 with updated diurnal correction factors compared to the
407 retrieval with HALOE version 19 correction factors. The archived HALOE version 19 retrieval
408 used correction factors from a diurnal calculation at 61 km for all mesospheric tangent altitudes
409 above. Since a partially corrected (version 19) retrieval was used as the basis, the contour levels
410 are negative and smaller in magnitude.

411

412 **4 Comparisons with other measurements**

Formatted: Font: 12 pt

413

414 It is of interest to see whether the correction to the retrieval of mesospheric ozone described
415 above can be validated by comparisons with other independent measurements. Mesospheric
416 ozone mixing ratios at SZA of 90° during sunrise and sunset have been measured by other solar
417 occultation experiments like HALOE and ACE-FTS. HALOE version 19 retrievals use
418 correction factors based on diurnal model calculation near the stratopause. An update to these
419 correction factors was discussed in Natarajan et al. (2005) but a modified version of the full
420 ozone dataset was not generated. As far as we know, the retrieval scheme of ACE-FTS does not
421 use any correction for twilight variations of mesospheric ozone. It should be emphasized that
422 comparisons with data from other solar occultation experiments do not necessarily provide a
423 robust independent validation of the need to make such corrections to reduce the bias in the
424 measurements.

Formatted: Font: 12 pt

Formatted: Font: 12 pt

Formatted: Font: 12 pt

Formatted: Font: 12 pt

Formatted: Font: 12 pt

425

426 MLS aboard the Aura satellite also provides vertical profiles of O₃ extending into the
427 mesosphere. MLS measurements occur twice a day, once in the early afternoon and the other
428 past midnight. Strode et al. (2022) have used the MLS data scaled with factors derived from
429 Goddard Earth Observing System (GEOS) model coupled with the Global Modeling Initiative
430 (GMI) chemistry mechanism for comparisons with SAGE III/ISS O₃ in the stratosphere. We
431 have done similar comparisons for a selected subset of the data in the lower mesosphere using
432 the results from the mesospheric diurnal model described earlier. We limited our attention to the
433 data in altitude range from 56 to 70 km. We used the information provided in the MLS-V5 data
434 quality document (Livesey et al., 2022) to properly screen the O₃ data. The vertical resolution for
435 MLS O₃ varies from 3 to 5.5 km in the lower mesosphere. The reported accuracy varies from 8%
436 at 0.21 hPa to 40% at 0.02 hPa. We used the MLS V-5 O₃ profiles from a 11.25° latitude band
437 centered at 11.25° S from June 13 to June 15 of 2021. The native units of MLS measurements
438 are mixing ratios on pressure levels. We used the MLS temperature and geopotential height data
439 to get O₃ concentrations on an altitude grid. We derived the mean and the standard deviation
440 profiles for both day and night MLS measurements. Results from diurnal model calculations
441 were used to convert MLS day and night measurements to SZA of 90° during sunrise and sunset
442 conditions. Figure 12 shows the O₃ concentration at sunrise based on MLS night data by
443 asterisks and that based on MLS day data by diamonds. The horizontal lines represent the
444 standard deviations at different altitudes. We also obtained the mean and standard deviation
445 profiles from SAGE III/ISS data the same latitude band and period in June 2021 like the selected
446 MLS data. The solid black line in the figure shows the mean sunrise profile from standard
447 retrieval and the standard deviation is represented by the yellow color band. The dashed black

Formatted: Font: 12 pt

Formatted: Font: 12 pt

Formatted: Font: 12 pt

Formatted: Font: 12 pt

Formatted: Font: 12 pt

Formatted: Font: 12 pt

Formatted: Font: 12 pt

Formatted: Font: 12 pt

Formatted: Font: 12 pt

448 line is the modified retrieval with the green band showing the standard deviation. The twilight
449 corrections to the mesospheric O₃ retrieval brings the profile in better agreement with that
450 derived from MLS day and night data. Above 68 km the MLS day measurements have large
451 variability, and the standard deviation is larger than the mean. Figure 13 shows the comparison
452 of the profiles for sunset conditions. The difference between the modified and the standard
453 retrievals is much smaller for the sunset conditions compared to the sunrise condition. Overall
454 SAGEIII/ISS mesospheric O₃ has a positive bias. The vertical resolution of SAGE III/ISS data is
455 about 0.7 km which is finer than the MLS vertical resolution. We found that the application of
456 the MLS O₃ averaging kernel to smooth the SAGE III/ISS data has a minimum impact on the
457 comparison.

Formatted: Font: 12 pt

458
459 There have been several ground-based microwave measurements of atmospheric O₃ and its
460 diurnal variations (Connor et al., 1994; Parrish et al., 2014; Sauvageat et al., 2022). The
461 microwave radiometry (MWR) in Switzerland (Sauvageat et al., 2022) provides data temporally
462 overlapping the SAGE III/ISS data. These data are from measurements made at 2 ground stations
463 and they extend into the mesosphere. The vertical resolution of ground based MWR is very
464 coarse in the lower mesosphere, about 17 km (Connor et al., 1994). Therefore SAGE III/ISS O₃
465 data should be convolved with the averaging kernels of MWR prior to comparisons. In addition,
466 MWR provides hourly data and, unless the local measurement time coincides with SZA of 90°
467 during sunrise and sunset, the data must be converted using factors based on diurnal model. We
468 feel that comparison with MWR data is outside the scope of this paper.

Formatted: Font: 12 pt

Formatted: Font: 12 pt

Formatted: Font: Not Bold

469

470 **5 Sunrise to Sunset Ratio**

471

472 Brühl et al. (1996), in their paper on HALOE O₃ channel validation, discussed the sunrise to

473 sunset differences in O₃ around 0.1 hPa (about 64 km). Mesospheric layers are under sunlit

474 conditions even at SZA slightly greater than 90° at dawn and dusk. As explained earlier, the

475 viewing geometry in solar occultation observations leads to an increase in the contribution of

476 overlying layers to the O₃ optical depth because O₃ concentrations corresponding to varying SZA

477 greater than 90° are seen along the LOS. We have noted that the impact is larger during sunrise

478 than sunset measurement. The sunrise to sunset O₃ concentration ratio becomes larger if the

479 diurnal variations along the LOS are not considered in the retrieval. Solar occultation

480 experiments occasionally offer the opportunity to approximately check this ratio as a test of

481 consistency of measurement and agreement with theory. This is possible when sunrise and

482 sunset orbits cross over each other within a reasonably short interval of time and physical

483 proximity. Such near coincidences are quite rare. We selected sunrise/sunset pairs of

484 measurements by SAGE III/ISS having tangent locations within 1.5° latitude, and 15° longitude

485 of each other and separated by a maximum of 36 hours. The effect of advection by the prevailing

486 westerly wind requires that the time and longitude differences are in the correct direction. There

487 are just 10 pairs of sunrise /sunset measurements in June 2021 that satisfy the above criteria, all

488 of them in low latitudes with a mean latitude of 10.46°S at sunrise and 10.27°S at sunset. The

489 mean of the sunrise to sunset ratios of O₃ concentrations for these 10 scans is shown in Figure

490 14. The solid line corresponding to the standard retrieval shows ratios greater than 1.1 above 60

491 km. The green color shade represents the standard deviation. The modified retrieval yields a ratio

492 shown by the dashed line decreasing from 1.01 at 60 km to lower values above. The horizontal

Deleted: ¶

Deleted: 4

Deleted: zenith angles

Deleted: zenith angles

Deleted: 1

Deleted: in the altitude range considered.

499 lines are the standard deviations. The asterisk symbols represent the ratio from the diurnal
500 model. The model value is in good agreement with the ratios from both the standard and
501 modified retrievals near 58 km but above this altitude there is some difference. The variation
502 with altitude in the model ratio is more like that shown by the modified retrieval. The modified
503 retrieval qualitatively reflects the pattern that photochemistry of O₃ suggests in this altitude
504 region. This comparison serves as an independent criterion to highlight the importance of
505 including the LOS twilight variations in the retrieval of mesospheric O₃ in solar occultation
506 measurements. We noticed that very few such pairs of measurements, which satisfied the criteria
507 we have chosen, occurred during other months in SAGE III/ISS data. We have also looked at the
508 latitudinally averaged sunrise and sunset data for June 2021 obtained for generating figures 9 and
509 10. For the latitude band centered at 11.25° S, the sunrise to sunset ratio as a function altitude
510 (not shown) is like Figure 14, which used only collocated data. The small sampling size of the
511 collocated pairs of data and regions of overlapping standard deviations seen in the Figure 14
512 make this at best an approximate comparison. Other independent measurements are needed to
513 verify the altitude variation of the ratio of sunrise to sunset O₃ concentrations.

Deleted: diamond

Deleted: and t

Deleted: decreasing model value with altitude is in qualitative agreement with the modified retrieval.

Deleted: , which satisfied the criteria we have chosen

Deleted: 8

Deleted: 9

Deleted: similar to

Deleted: 1

Deleted: 1

515 6 Summary

Deleted: 5

516
517 Photochemically induced changes in species concentration at twilight can cause asymmetries in
518 the distribution along the LOS of a solar occultation observation, variations that must be
519 considered in the retrieval algorithm. Prominent among the species that need corrections for
520 twilight variations are NO and NO₂ in the stratosphere and O₃ in the mesosphere. The SAGE
521 III/ISS instrument uses the measurements in the short-wave Hartley-Huggins band to get

533 mesospheric O₃ profiles. The standard retrieval procedure does not consider the LOS variations
534 in O₃ caused by photochemistry. This study describes a procedure to use results from diurnal
535 photochemical model simulations to develop correction factors for different altitudes, latitudes,
536 and months. These factors were used along with the archived SAGE III/ISS mesospheric O₃ data
537 for selected time periods to obtain modified O₃ profiles. For the month of June 2021, it is shown
538 that neglecting the diurnal variations can result in nearly 50% overestimation of O₃ at 64 km and
539 low latitudes. An approximate retrieval using the transmission data from SAGE III/ISS also
540 indicates similar behavior in the profiles obtained with and without diurnal corrections. The
541 retrievals were repeated for January 2021 to study the seasonal impact. Larger differences are
542 generally seen near 70 km in high latitude winter hemisphere, and this is most likely due to a
543 combination of very low O₃ concentrations, large twilight correction factors, and large
544 uncertainties in the data. The results from this study are in good agreement with those obtained
545 for the retrieval of HALOE mesospheric O₃ data.

Deleted: over 3

Deleted: seen

Deleted: between

Deleted: and 80

546
547 SAGE III/ISS data include a few nearly collocated sunrise and sunset measurements, mostly in
548 the low latitudes and about a day apart. There are 10 pairs of such sunrise and sunset
549 measurements in June 2021. An analysis of the sunrise to sunset ratio profile from these data
550 indicates that the retrievals that include the diurnal variations show qualitatively better agreement
551 with theoretical prediction.

Deleted: 1

Deleted: We note that dynamical causes such as diurnal tides may also introduce variations in the sunrise to sunset O₃ ratio especially in the low latitudes. The diurnal corrections described for occultation retrievals depend mainly on the short period variations around 90° solar zenith angle and dynamical impacts will not be significant compared to the photochemical effects.

553 Data Availability

554 SAGE III/ISS version 5.2 data is available from [https://asdc.larc.nasa.gov/project/SAGE%20III-](https://asdc.larc.nasa.gov/project/SAGE%20III-ISS/g3bssp_52)
555 [ISS/g3bssp_52](https://asdc.larc.nasa.gov/project/SAGE%20III-ISS/g3bssp_52). MLS O₃ data are available from <https://disc.gsfc.nasa.gov/>. O₃ twilight ratios

Deleted: The

569 used in this study are available from the author. They can also be obtained from any diurnal
570 photochemical model of the mesosphere.

571

572 **Author Contribution**

573 MN conducted the photochemical model calculations, SAGE III/ISS O₃ retrievals, and the
574 analyses described in the study, and he wrote the manuscript. RD and DF provided information
575 and guidance on the use of SAGE III/ISS mesospheric O₃ data as well as comments on the
576 manuscript.

577

578 **Competing Interests**

579 The authors declare that there is no competing interest for this study.

580

581 **Acknowledgements**

582 SAGE III/ISS data used in this study were obtained from the NASA Langley Research Center
583 Atmospheric Science Data Center. MN carried out this work while serving as a Distinguished
584 Research Associate of the Science Directorate at NASA Langley Research Center. [MN thanks](#)
585 [Ellis Remsberg for reading and commenting on the draft version of this manuscript.](#)

586

587 **References**

588

589 Bogumil, K., Orphal, J., Homann, S., Voigt, P., Spietz, O., Fleischmann, A., Vogel, M.,
590 Hartmann, H., Bovensmann, J., Frerick, J., and Burrows, J.: Measurements of molecular
591 absorption spectra with the SCIAMACHY pre-flight model: instrument characterization and

592 reference data for atmospheric remote sensing in the 230-2380 nm region, *J. Photochemistry and*
593 *Photobiology A: Chemistry*, Vol 157, No. 2-3, 167-184, 2003.

594 Boughner R. E., Larsen, J. E., and Natarajan., M.: The influence of NO and ClO variations at
595 twilight on the interpretation of solar occultation measurements, *Geophys. Res. Lett.*, 7, 231 –
596 234, 1980.

597 Brohede, S. M., Haley, C. S., McLinden, C. A., Sioris, C. E., Murtagh, D. P., Petelina, S. V.,
598 Llewellyn, E. J., Bazureau, A., Goutail, F., Randall, C. E., Lumpe, J. D., Taha, G., Thomasson,
599 L. W., and Gordley, L. L.: Validation of Odin/OSIRIS stratospheric NO₂ profiles, *J. Geophys.*
600 *Res.-Atmos.*, 112, D07310, <https://doi.org/10.1029/2006JD007586>, 2007.

601 Brühl, C., Drayson, S. R., Russell III, J. M., Crutzen, P. J., McInerney, J. M., Purcell, P. N.,
602 Claude, H., Gernandt, H., McGee, T. J., McDermid, I. S., and Gunson, M. R.: Halogen
603 Occultation Experiment ozone channel validation, *J. Geophys. Res.*, Vol. 101, NO. D6, 10,217 -
604 10,240, 1996.

605 [Connor, B. J., Siskind, D. E., Tsou, J. J., Parrish, A., and Remsberg, E. E.: Ground-based](#)
606 [microwave observations of ozone in the upper stratosphere and mesosphere, *J. Geophys. Res.*,](#)
607 [vol 99, No. D8, 16,757-16,770, 1994.](#)

608 [Dubé, K., Bourassa, A., Zawada, D., Degenstein, D., Damadeo, R., Flittner, D., and Randel, W.:](#)
609 Accounting for the photochemical variation in stratospheric NO₂ in the SAGE III/ISS solar
610 occultation retrieval, *Atmos. Meas. Tech.*, 14, 557 – 566, [https://doi.org/10.5194/amt-14-557-](https://doi.org/10.5194/amt-14-557-2021)
611 [2021](https://doi.org/10.5194/amt-14-557-2021), 2021.

612 Gordley, L. L., Russell III, J. M., Mickley, L. J., Frederick, J. E., Park, J. H., Stone, K. A.,

613 [Beavee, G. M., McInerney, J. M., Deaver, L. E., Toon, G. C., Murcray, F. J., Blatherwick, R. D.,](#)
614 Gunson, M. R., Abbatt, J. P. D., Mauldin III, R. L., Mount, G. H., Sen, B., and Blavier, J. F.:

Deleted: c

Deleted: Beaver

617 Validation of nitric oxide and nitrogen dioxide measurements made by the Halogen Occultation
618 Experiment for UARS platform, J. Geophys. Res.-Atmos., 101,10241–10266, 1996.

619 JPL Publication 19-5, Chemical Kinetics and Photochemical Data for Use in Atmospheric
620 Studies, Evaluation Number 19, <https://jpldataeval.jpl.nasa.gov/pdf/NASA->
621 [JPL%20Evaluation%2019-5.pdf](https://jpldataeval.jpl.nasa.gov/pdf/NASA-JPL%20Evaluation%2019-5.pdf), 2020.

622 [Livesey, N. J., Read, W. G., Wagner, P. A., Froidevaux, L., Santee, M. L., Schwartz, M. J.,](#)
623 [Lambert, A., Millan Valle, L. F., Pumphrey, H. C., Manney, G. L., Fuller, R. A., Jarot, R. F.,](#)
624 [Knosp, B. W., and Lay, R. R.: Earth Observing System \(EOS\) Aura Microwave Limb Sounder](#)
625 [\(MLS\) Version 5.0x Level 2 and 3 data quality and description document, JPL D-105336 Rev B,](#)
626 [2022.](#)

627 McCormick, M. P., Lei, L., Hill, M. T., Anderson, J., Querel, R., and Steinbrecht, W.: Early
628 results and validation of SAGE III-ISS ozone profile measurements from onboard the
629 International Space Station, Atmos. Meas. Tech., 13, 1287-1297, [https://doi.org/10.5194/amt-13-](https://doi.org/10.5194/amt-13-1287-2020)
630 [1287-2020](https://doi.org/10.5194/amt-13-1287-2020), 2020.

631 Natarajan, M., Deaver, L. E., Thompson, E., and Magill, B.: Impact of twilight gradients on the
632 retrieval of mesospheric ozone from HALOE, J. Geophys. Res., Vol. 110,
633 doi:10.1029/2004JD005719, 2005.

634 Newchurch, M. J., Allen, M., Gunson, M. R., Salawitch, R. J., Collins, G. B., Huston, K. H.,
635 Abbas, M. M., Abrams, M. C., Chang, A. Y., Fahey, D. W., Gao, R. S., Irion, F. W.,
636 Loewenstein, M., Manney, G. L., Michelson, H. A., Podolske, J. R., Rinsland, C. P., and Zander,
637 R.: Stratospheric NO and NO₂ abundances from ATMOS Solar-Occultation Measurements,
638 Geophys. Res. Lett., 23, 2373-2376., <https://doi.org/10.1029/96GL01196>, 1996.

Deleted: , 2020

640 [Parrish, A., Boyd, I. S., Nedoluha, G. E., Bhartia, P. K., Firth, S. M., Kramarova, N. A., Connor,](#)
641 [B. J., Bodeker, G. E., Froidevaux, L., Shiotani, M., and Sakazaki, T.: Diurnal variations of](#)
642 [stratospheric ozone measured by ground-based microwave remote sensing at the Mauna Loa](#)
643 [NDACC site: measurement validation and GEOSCCM model comparison, Atmos. Chem. Phys.,](#)
644 [14, 7255-7222, www.atmos-chem-phys.net/14/7255/2014/doi:10.5194/acp-14-7255-2014, 2014](#)
645 [Remsberg, E., Damadeo, R., Natarajan, M., and Bhatt, P.: Observed responses of mesospheric](#)
646 [water vapor to solar cycle and dynamical forcings, J. Geophys. Res., 123 \(7\), 3830-3843,](#)
647 [https://doi.org/10.1002/2017JD028029, 2018.](https://doi.org/10.1002/2017JD028029)

648 Russell III, J. M., Farmer, C. B., Rinsland, C. P., Zander, R., Froidevaux, L., Toon, G. C., Gai,
649 B., Shaw, J., and Gunson, M.: Measurements of Odd Nitrogen Compounds in the Stratosphere
650 by the ATMOS Experiment on Spacelab 3, J. Geophys. Res., Vol 3, D2, 1718-1736, 1988.

651 [Sauvageat, E., Barras, E. M., Hocke, K., Haeferle, A., and Murk, A.: Harmonized retrieval of](#)
652 [middle atmospheric ozone from two microwave radiometers in Switzerland,](#)
653 [https://doi.org/10.5194/amt-2022-212, 2022](https://doi.org/10.5194/amt-2022-212)

654 SAGE III Algorithm Theoretical Basis Document (ATBD) Solar and Lunar Algorithm, LaRC
655 475-00-109, Version 2.1, [https://eosps.gsfc.nasa.gov/sites/default/files/atbd/atbd-sage-solar-](https://eosps.gsfc.nasa.gov/sites/default/files/atbd/atbd-sage-solar-lunar.pdf)
656 [lunar.pdf](https://eosps.gsfc.nasa.gov/sites/default/files/atbd/atbd-sage-solar-lunar.pdf), 2002

657 SAGE III/ISS Data Products User's Guide, Version 3.0, <https://asdc.larc.nasa.gov/documents/sageiii-iss/guide/DPUG-G3B-2-0.pdf>, 2021.

658 [Strode, S. A., Taha, G., Oman, L. D., Damadeo, R., Flittner, D., Schoeberl, M., Sioris, C. E., and](#)
660 [Stauffer, R.: SAGE III/ISS ozone and NO₂ validation using diurnal scaling factors,](#)
661 <https://doi.org/10.5194/amt-15-6145-2022>, Atmos. Meas. Tech., 15, 6145-6161, 2022

Field Code Changed

Deleted: , 2002

Deleted: 2021.

664 Wang, H. J. R., Damadeo, R., Flittner, D., Kramarova, N., Taha, G., Davis, S., et al.: Validation
665 of SAGE III/ISS solar occultation ozone products with correlative satellite and ground-based
666 measurements, J. Geophys. Res., 125, e2020JD032430. <https://doi.org/10.1029/2020JD032430>,
667 [2020](#).
668 [Yue, J., Russell III, J., Gan, Q., Wang, T., Rong, P., Garcia, R., and Mlynczak, M.:Increasing](#)
669 [water vapor in the stratosphere and mesosphere after 2002, Geophys. Res. Lett., 46, 13,452-](#)
670 [13,460. https://doi.org/10.1029/2019GL084973, 2019.](#)

671

672 **Appendix**

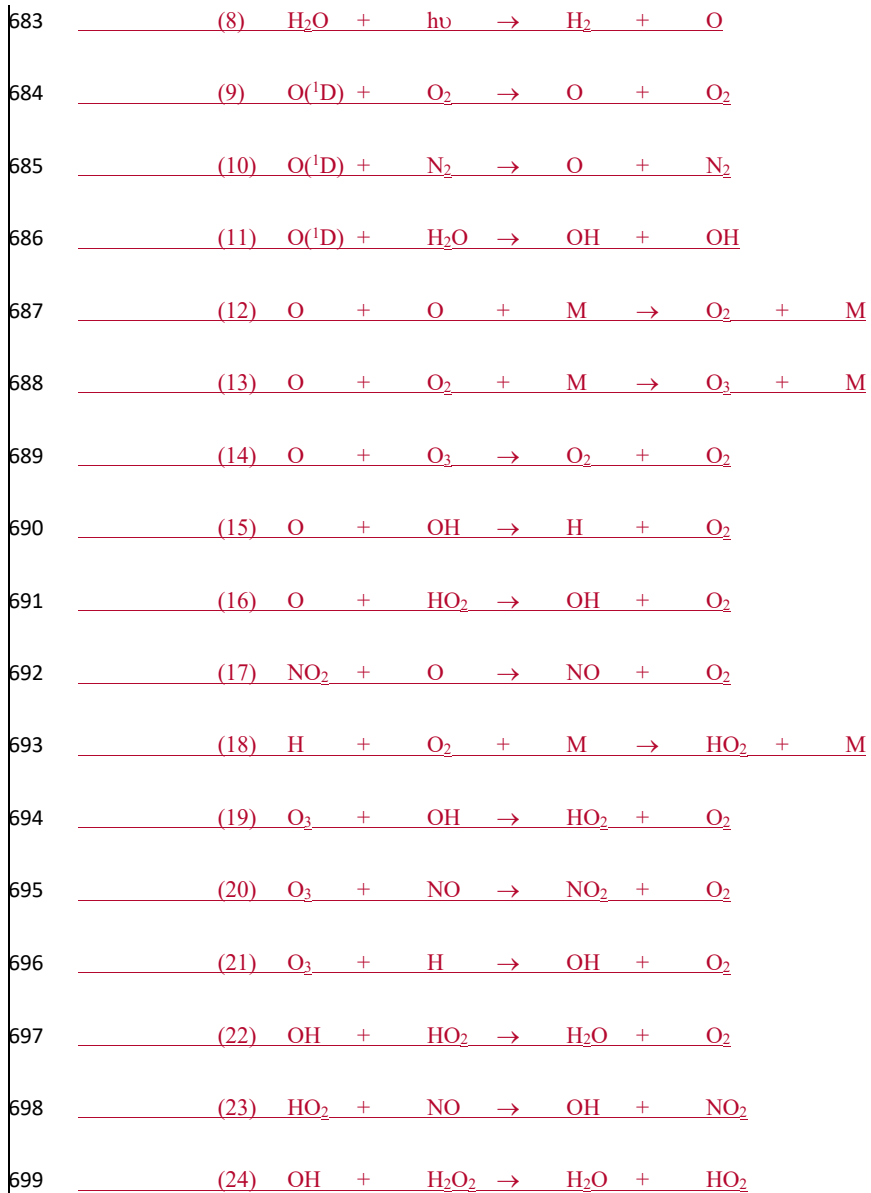
673

674 **Photochemical reactions considered in the mesospheric diurnal model:**

Formatted: Indent: First line: 0.5"

675



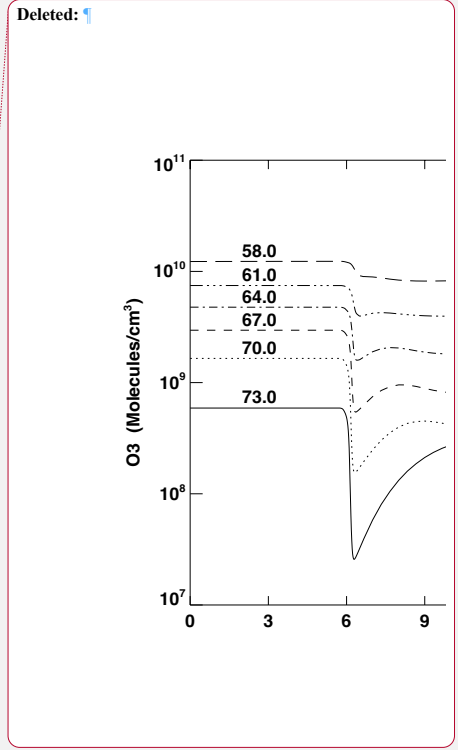
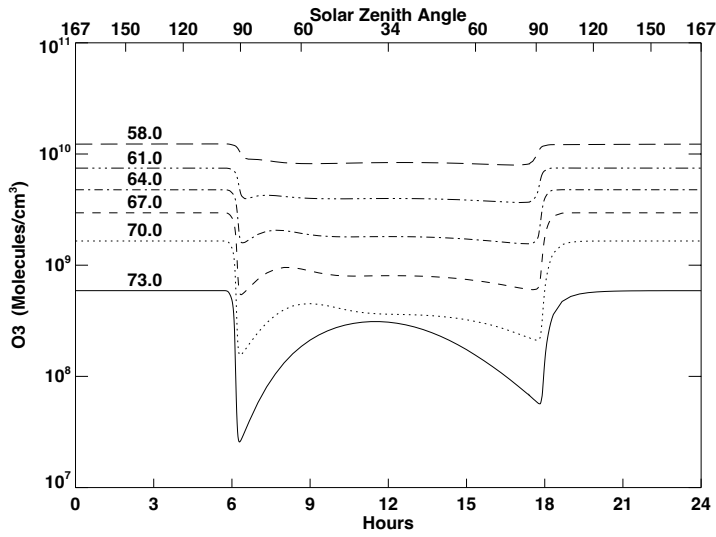




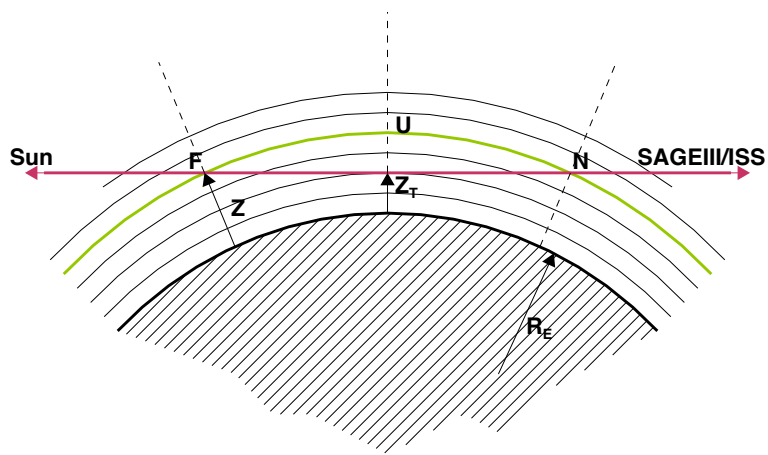
710 Deleted: -----Page Break-----

711

712



714
 715
 716 Figure 1. Diurnal variation in O₃ at 11.25°S in June at altitudes from 58 to 73 km. 0 hours
 717 denote midnight. The upper X axis shows the variation of SZA.

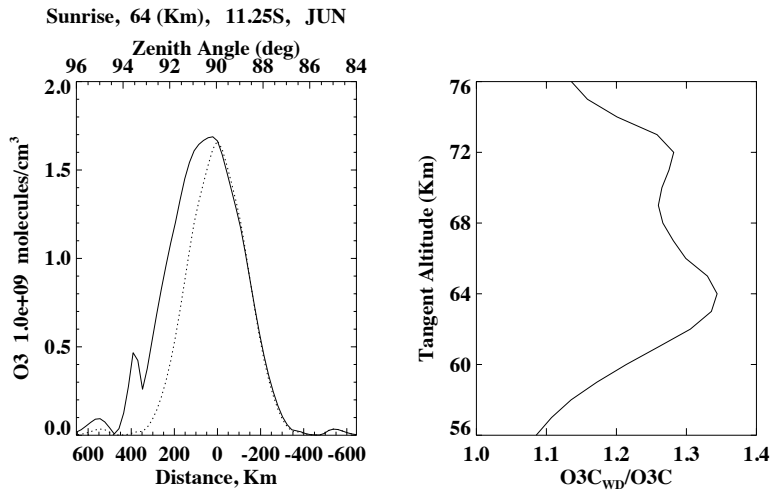


721

722 Figure 2. Schematic representation of the solar occultation measurement. Z_T is the tangent
 723 altitude, red line is the LOS, Z is the altitude of a layer above the tangent altitude, F (towards
 724 sun) and N (towards SAGE III/ISS) are the points of intersection of layer at Z with the LOS, and
 725 R_E is the earth radius.

726

Deleted: ¶



728

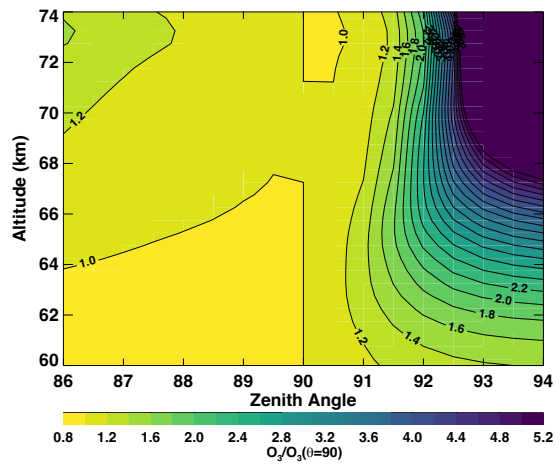
729 Figure 3. (Left) O₃ concentration along the LOS for a tangent altitude of 64 km at 11.25°S
 730 latitude in June. Solid line shows O₃ with diurnal variations and the dotted line represents O₃
 731 without diurnal variations. The X-axis represents the distance along the LOS relative to the
 732 tangent point with positive direction towards the instrument and negative direction towards the
 733 Sun. The upper axis shows the corresponding SZA. (Right) Ratio of the O₃ column along the
 734 LOS with appropriate diurnal variations to the O₃ column without diurnal variations, plotted as a
 735 function of altitude at 11.25°S in June.

736

737

Deleted: ¶

740



741

742 Figure 4. Ozone twilight ratio, defined as O_3 at solar zenith angle θ/O_3 at $\theta=90^\circ$, as a function of

743 SZA and altitude for sunrise in June and 11.25°S latitude.

744

745

Deleted: ¶

Deleted: zenith angle

Formatted: Font: (Default) Times New Roman

Formatted: Font: (Default) Times New Roman

Formatted: Font: (Default) Times New Roman

Formatted: Font: (Default) Times New Roman

Formatted: Font: (Default) Times New Roman

Formatted: Font: (Default) Times New Roman

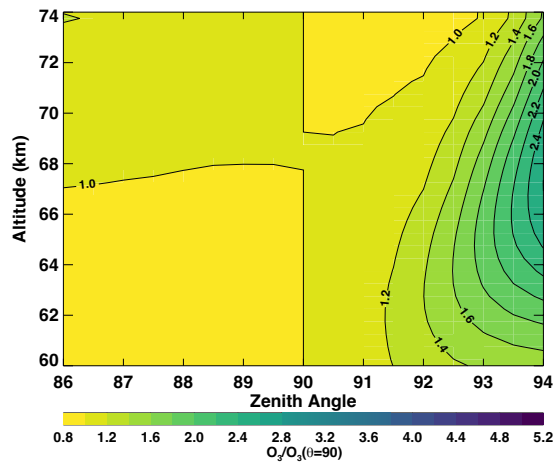
Formatted: Font: (Default) Times New Roman

Deleted: zenith angle

Formatted: Font: (Default) Times New Roman

Formatted: Font: (Default) Times New Roman

Deleted: ¶



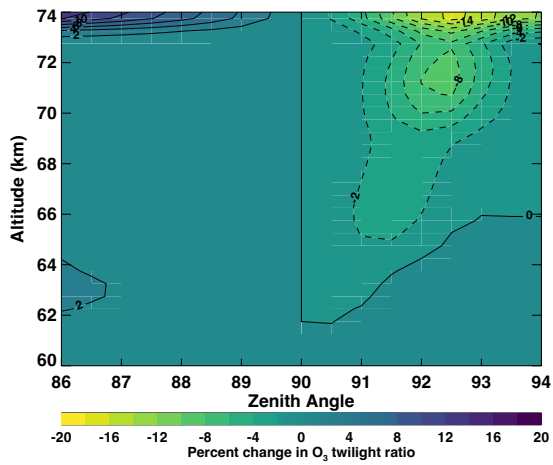
752

753 Figure 5. Same as Figure 4 for sunset conditions

754

Deleted: ¶

Formatted: Font: (Default) Times New Roman



Deleted: ¶

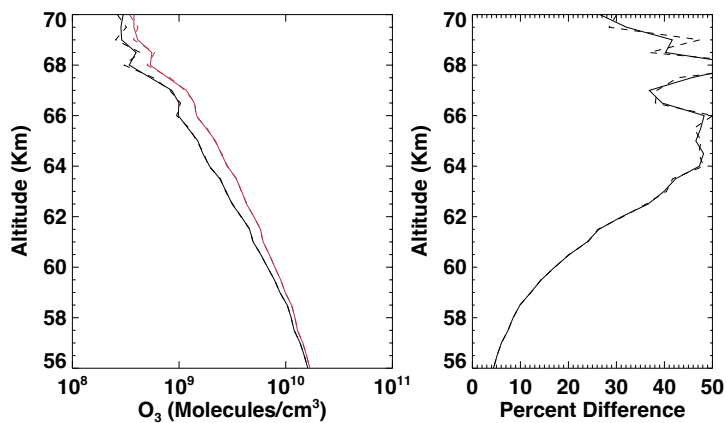
757

758 Figure 6. Percent change in the O₃ twilight ratio shown in Figure 4 when the H₂O in the diurnal
 759 model is increased by 25% at all altitudes. This figure corresponds to sunrise at 11.25° S in June.

Formatted: Font: (Default) Times New Roman

Formatted: Font: (Default) Times New Roman

Formatted: Font: (Default) Times New Roman



761

762 Figure 7. SAGE III/ISS sunrise O₃ for a sunrise event on June 14, 2021 (Event ID
 763 2021061438SR). (Left panel) Red solid line shows the standard SAGE III retrieval, and the black
 764 solid line represents the retrieval including the diurnal variations along LOS. The dashed lines
 765 represent the retrievals using the transmission data, the red color for the standard retrieval and
 766 the black denoting the retrieval with diurnal corrections. (Right panel) Percent difference
 767 between the standard retrieval and the one with diurnal corrections; solid line using the archived
 768 standard retrieval of O₃ concentration, and the dashed line based on the approximate retrieval
 769 using the transmission data.

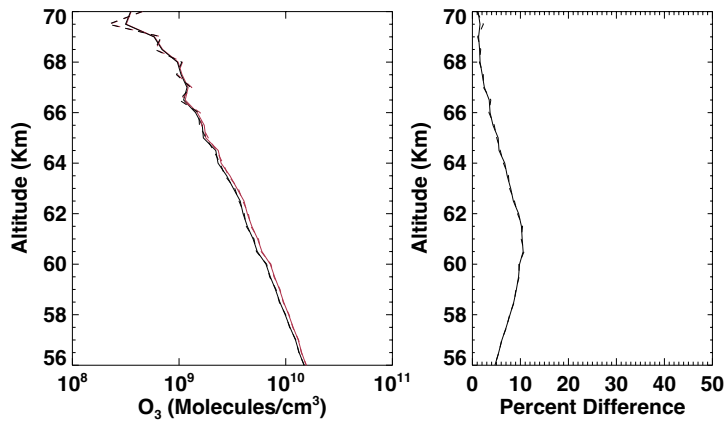
770

Deleted: ¶

Deleted: 6

Formatted: Font: (Default) Times New Roman

Deleted: ¶

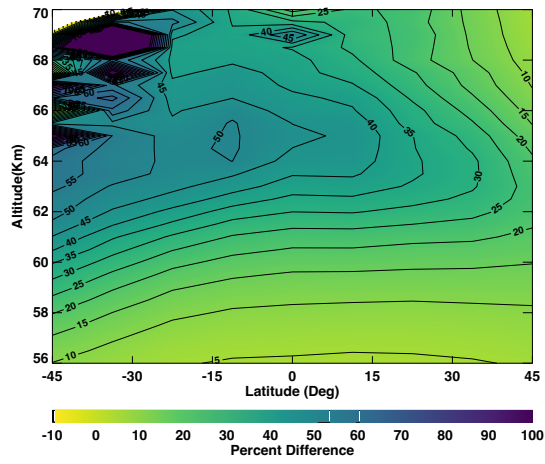


774

775 Figure 8. Same as Figure 7 but for a sunset event (Event ID 2021061515SS) closer to the sunrise
 776 event shown in Figure 7.

777

- Deleted: ¶
- Deleted: 7
- Deleted: 6
- Formatted: Font: (Default) Times New Roman
- Deleted: 6
- Deleted: ¶
- ¶
- ¶



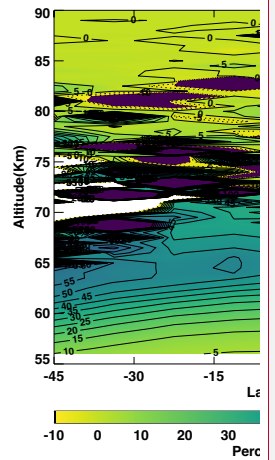
785

786 Figure 9. Latitudinal average of the percent difference in sunrise O₃ between the standard
 787 (archived) retrieval and a retrieval including diurnal variations along the LOS, as a function of
 788 latitude and altitude for June 2021.

789

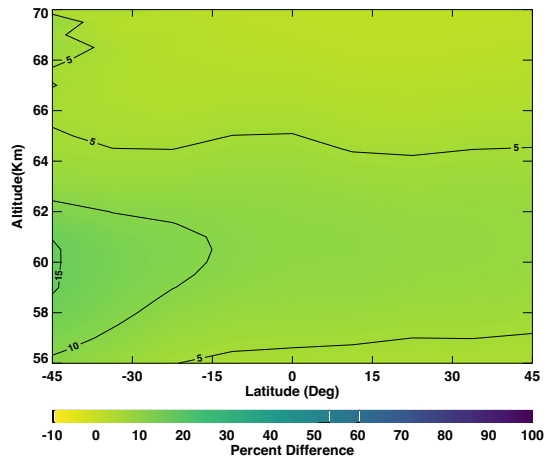
790

Deleted: ¶



Deleted: 8

Formatted: Font: (Default) Times New Roman

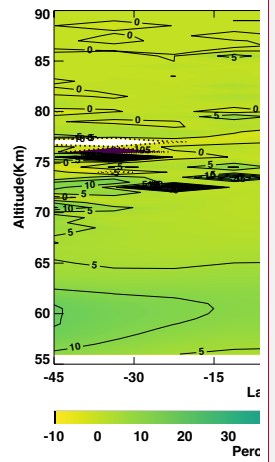


796

797 Figure 10. Same as Figure 9, but for sunset conditions.

Deleted: ¶

¶

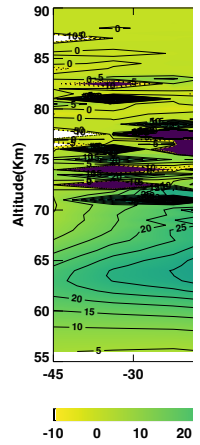
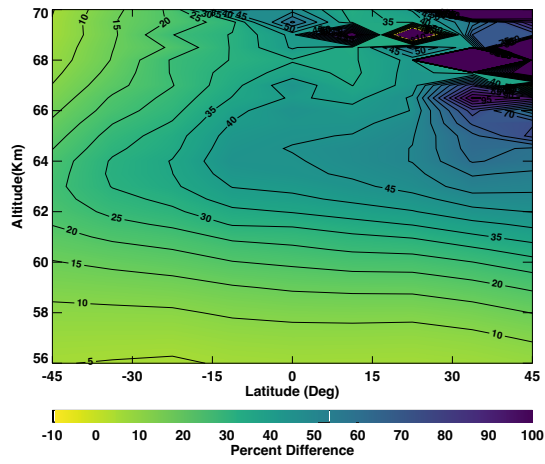


Deleted: ¶

¶

Deleted: 9

Deleted: 8



805

806 Figure 11. Same as Figure 9, but for January 2021.

807

808

Deleted:

Deleted: ¶

Deleted: ¶

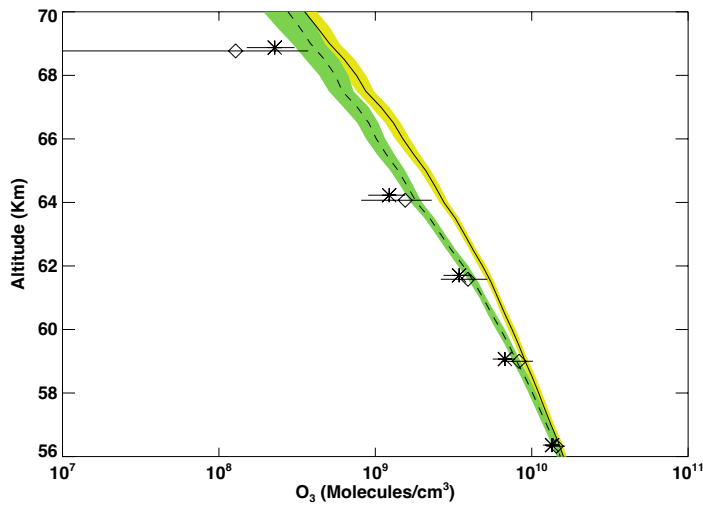
Deleted: 0

Deleted: 8

Formatted: Font: (Default) Times New Roman

Deleted: ¶

¶



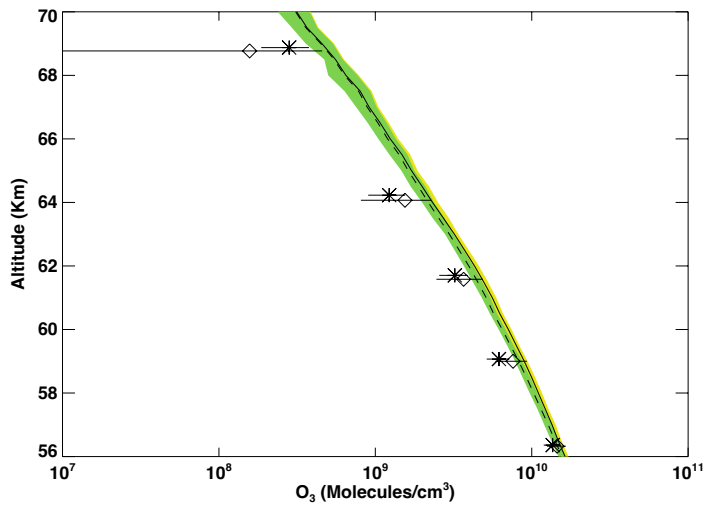
816
 817 Figure 12. Comparison of sunrise SAGE III/ISS and MLS mesospheric O₃ zonal mean at 11.25°
 818 S in June 2021. Solid line – mean of SAGE III/ISS standard retrieval with the standard deviation
 819 shown by the yellow shade; Dashed line – mean of SAGE III/ISS modified retrieval with the
 820 standard deviation shown by the green shade; Asterisks – mean MLS night data scaled to
 821 sunrise; Diamonds – mean MLS day data scaled to sunrise; Horizontal lines represent the
 822 standard deviations.

823

Formatted: Font: (Default) Times New Roman, Not Superscript/ Subscript

Deleted: ¶

Formatted: Font: (Default) Times New Roman, Not Superscript/ Subscript



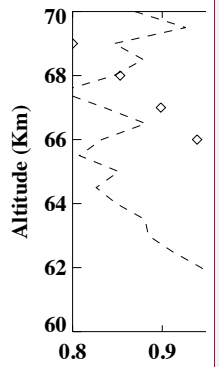
825

826

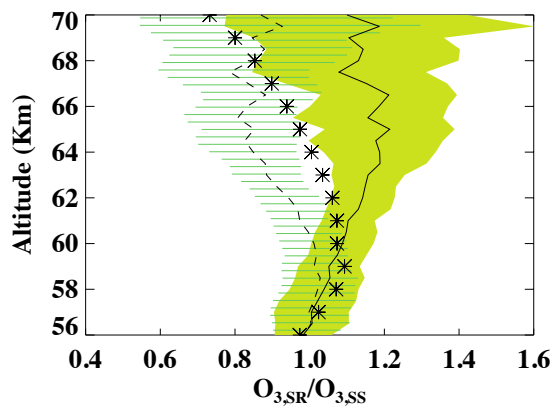
827

Figure 13. Same as Figure 12 but for sunset condition.

Formatted: Font: (Default) Times New Roman, Not Superscript/ Subscript



Deleted:



829

830 Figure 14. Vertical profile of O₃ sunrise to sunset ratio in June 2021. Nearly collocated 10 pairs

831 of sunrises (mean latitude 10.46°S) and sunsets (mean latitude 10.27°S) data are used for this

832 plot. Solid line shows the mean ratio from standard (archived) retrieval and the green shade

833 represents the standard deviation; Dashed line shows the mean ratio from the retrieval including

834 diurnal variations along the LOS and the horizontal lines represent the standard deviation. The

835 asterisk symbols are the ratios from diurnal photochemical calculations at 11.25°S for June.

Formatted: Font: (Default) Times New Roman

Deleted: 1

Formatted: Font: (Default) Times New Roman

Formatted: Font: (Default) Times New Roman

Formatted: Font: (Default) Times New Roman

Formatted: Font: (Default) Times New Roman

Deleted: represent

Formatted: Font: (Default) Times New Roman

Deleted: , and the d

Formatted: Font: (Default) Times New Roman

Formatted: Font: (Default) Times New Roman

Deleted: diamond

Formatted: Font: (Default) Times New Roman

Formatted: Font: (Default) Times New Roman

Formatted: Font: (Default) Times New Roman